Title: The contrasting roles of nitric oxide drive microbial community organization as a function of oxygen presence

Steven A. Wilbert[1] and Dianne K. Newman[1,2,*]

Contact information:

[1] Division of Biology and Biological Engineering, California Institute of Technology, Pasadena, California, USA, 91125

[2] Division of Geological and Planetary Sciences, California Institute of Technology, Pasadena, California, USA, 91125

[*]**Correspondence:**

Lead Contact: Dianne K. Newman

1200 E. California Blvd., Mail code 147-75

Pasadena, CA 91125

Telephone: 626-395-3543

Email: dkn@caltech.edu

Keywords: Polymicrobial communities, redox active metabolites, metabolic cross-feeding, nitric oxide, nitrate, denitrification, spatial organization, microenvironment, oxygen gradients, *Pseudomonas aeruginosa*

Summary

Microbial assemblages are omnipresent in the biosphere, forming communities on the surfaces of roots, rocks, and within living tissues. These communities can exhibit strikingly beautiful compositional structures, with certain members reproducibly occupying particular spatiotemporal microniches. Despite this reproducibility, we lack the ability to explain these spatial patterns. We hypothesize that certain spatial patterns in microbial communities may be explained by the exchange of redox-active metabolites whose biological function is sensitive to microenvironmental gradients. To test this, we developed a simple community consisting of synthetic *Pseudomonas aeruginosa* strains with a partitioned denitrification pathway: a strict consumer and strict producer of nitric oxide (NO), a key pathway intermediate. Because NO can be both toxic or beneficial depending on the amount of oxygen present, this system provided an opportunity to investigate whether dynamic oxygen gradients can tune metabolic cross-feeding

and fitness outcomes in a predictable fashion. Using a combination of genetic analysis, controlled growth environments and imaging, we show that oxygen availability dictates whether NO cross-feeding is deleterious or mutually beneficial, and that this organizing principal maps to the microscale. More generally, this work underscores the importance of considering the contrasting and microenvironmentally tuned roles redox-active metabolites can play in shaping microbial communities.

Introduction

Given the diversity of microbial metabolic strategies and that microbes rarely live alone, the potential for metabolic interactions is vast [1]. Metabolic interactions can be positive or negative and can have profound effects on the surrounding environment, from contributing to nutrient flux to stimulating the immune system of an infected animal or plant. Numerous ecological models have been developed to better understand how such interactions influence the growth of a community [2–4]. However, these models typically focus on simple growth kinetics involving a shared or exchanged beneficial metabolite and do not consider how changing microenvironments over small spatial scales might influence the initiation and/or quality of the interaction. Yet it is a well-documented ecological phenomenon that microbes are confronted with environmental changes that can tune these interactions, such as shifting oxygen concentrations, in both space and time [5–8]. How such spatiotemporal environmental changes impact the function of exchanged metabolites is often overlooked in these models.

Diffusible, redox-active metabolites, be they organic or inorganic, are particularly relevant to consider in this context, as these molecules' reactivity is highly sensitive to local chemistry. Certain redox-active metabolites have the potential to be both toxic (i.e. generate reactive oxygen species under oxic conditions) or beneficial (i.e. contribute to energy conservation under anoxic conditions), thereby having the potential to play dynamic roles in the development of a microbial community [9]. Such contrasting effects may be particularly important when the metabolite is an intermediate in a common metabolic pathway. For example, if two microbes are reliant on each other for growth due to an intermediate that can be toxic to the producer but is essential for the consumer, it stands to reason that their growth and subsequent environmental impact will depend on microenvironmental conditions that affect the properties of the exchanged intermediate. The potential for variable local interactions due to shifting environmental gradients would therefore be expected to determine when, where, and how certain microbial interactions would manifest spatiotemporally.

As a step toward testing this hypothesis, we sought to create a simple synthetic model system in which to explore the effect of the microenvironment on the interactions between two bacterial partners linked via an exchanged redox-active metabolite. Four criteria guided our development of such a system. First, we required that the metabolite be “agathokakological”, a word derived from Greek roots meaning “composed of good and evil”. In other words, a metabolite that is predictably contrasting: beneficial or harmful according to its environmental context. Second, we needed to be able to measure and perturb the most important environmental parameter—oxygen—that affects its physiological impacts. Third, we aimed to control the production and utilization of this metabolite via the generation of mutant strains from an isogenic background in order to focus strictly on the capacity to make or use the metabolite. Finally, we sought a metabolic exchange that is of broad ecological relevance across many environments.

The exchange of nitric oxide (NO) met all of our criteria. NO is known in both the eukaryotic and microbial worlds as a potent signaling molecule and a highly reactive nitrogen species that can damage a variety of cellular components [10]. In the absence of oxygen, NO is toxic at high concentrations by antagonizing Fe-S centers and causing DNA damage; yet in the presence of oxygen, much lower levels of NO can be toxic due the generation of peroxynitrite [11,12]. Microbes have numerous mechanisms to deal with low levels of NO toxicity such as flavohemoglobin proteins (Fhp) that can reduce NO to nitrous oxide (N_2O) or mediate its oxidation to nitrate (NO_3^-) depending on the environment [13,14], and other dioxygenases can sequester NO [15,16]. However, as its concentration rises, and if producing cells or neighbors are unable to reduce it to nitrous oxide (N_2O), it reaches toxic levels and leads to local growth inhibition or death [17,18].

NO production is also a landmark step in denitrification, where the soluble substrate nitrite (NO_2^-) is reduced to gaseous NO. Denitrification *sensu stricto* plays a critical role in the loss of nitrogen in soils [19–21]. If an organism contains a full pathway to sequentially reduce nitrate (NO_3^-) > NO_2^- > NO > N_2O > nitrogen gas (N_2), harmless N_2 will be released into the environment where it can eventually become recycled by nitrogen fixing species [22]. However, the complete reduction of NO_3^- to N_2 may occur as a polymicrobial community effort in which different members contain only a subset of the denitrification pathway [23–26]. Synthetic pseudomonads have previously been shown to exchange nitrite under strictly anoxic conditions, leading to predictable spatial patterns that are sensitive to pH-dependent abiotic nitrite reduction to toxic nitrogen species [27–30]. In an independent study, environmental isolates that naturally differ in their possession of denitrification genes were used to create a model that predicted

102 interactions via denitrification intermediates[23]; yet, in this case, NO production was only
103 considered for its potential toxicity rather than any potential for energy conservation. Because
104 PA uses a NO reductase that does not directly contribute to proton translocation (qNor), it is
105 often considered only for its detoxifying potential [10]. However, physiological studies have shown
106 that NO reduction in other, qNor-containing strains can contribute to ATP synthesis as the sole
107 terminal electron acceptor (TEA) [31,32]. To our knowledge, the ability for NO to be exchanged
108 between cells in a manner that supports growth has not been demonstrated.
109 Here, we utilized the denitrifying organism *P. aeruginosa* strain PA14 to test the
110 hypothesis that the spatial interactions of strains exchanging NO can be predictably altered as a
111 function of oxygen in the microenvironment. *P. aeruginosa* is a cosmopolitan organism,
112 notorious for being an opportunistic human pathogen, but is also found in sediments and soils
113 [13]. *P. aeruginosa* is also a classic denitrifier that encodes all enzymes necessary for the
114 complete reduction of nitrate to nitrogen gas and can be easily genetically manipulated,
115 permitting the creation of a synthetic NO cross-feeding community. Our findings provide a
116 conceptual lens through which to interpret more complex microbial community patterning in
117 nature and disease involving the exchange of redox active metabolites.
118
119 **Results**
120 **Design and characterization of a synthetic NO cross-feeding community.**
121 The PA14 genome contains a full suite of respiratory enzymes for the complete
122 dissimilatory reduction of NO_3^- to N_2 (Nar, Nap, Nir, Nor, Nos) (Figure 1A) [13]. Previous studies
123 have shown that these steps occur sequentially and thus intermediates can build up and leak
124 from the cell [33]. Because the PA14 NO reductase (Nor) does not directly contribute to proton
125 translocation and in fact requires the consumption of protons for its reaction, it is often
126 dismissed for contributing to energy conservation. However, if we trace the flow of electrons
127 (Figure 1B, gray dashed lines) originating from the oxidation of NADH by the Nuo NADH
128 dehydrogenase, through the quinone pool to the bc_1 complex, a total of six protons are
129 translocated prior to NO reduction [34]. If we account for the two protons consumed by the
130 reduction of two NO molecules to one N_2O and one H_2O (Figure 1B, solid line), four protons still
131 remain per NADH oxidized that could contribute to the proton motive force. Electron flow to the
132 N_2O reductase (Nos), which reduces N_2O to N_2, is also thought to follow the same pathway [34].
133 Thus, when considering the full electron transport chain, we expect for each NADH oxidized, a
134 net of $4H^+$ to be translocated per NO reduced all the way to N_2. Accordingly, there is good

135 reason to expect NO to be able to support sufficient energy conservation to power growth under
136 anoxic conditions, provided its toxicity under these conditions is managed.
137 To determine how the wild type (WT) PA14 strain responds to NO exposure, we
138 incubated it with a common NO donor molecule called DEA NONOate under both anoxic and
139 oxic conditions (Figure 1C). DEA NONOate releases 1.5 moles of NO per mole of parent
140 molecule. WT cells were grown to mid-exponential phase, washed into anoxic buffer (pH 7.4)
141 with and without a final concentration of 50μM NO donor (~75 μM NO). This concentration was
142 chosen to exceed that which has been shown to be tolerated by NO reductase (Nor) deficient
143 mutants (~15 μM) with the expectation that the WT strain could detoxify using its Nor [16].
144 Cultures were incubated at room temperature in an anoxic glove box for one hour (donor half-
145 life ~16 minutes). After incubation, cultures were washed in fresh anoxic buffer and plated for
146 colony forming units (CFUs) which revealed a 50% NO killing compared to an untreated control
147 (Figure 1C). Next, we hypothesized that incubating cells with NO donor under oxic conditions
148 would increase the toxic effects. After repeating this experiment under a normal atmosphere,
149 NO exposure killing increased to 90% of the population (Figure 1C). These results suggest that
150 NO as the sole TEA has the potential to contribute to energy conservation if certain conditions
151 are met: that its concentration be maintained in the sub 75 μM range and that oxygen not be
152 present in the microenvironment.
153 To generate NO at the microscale, we partitioned the PA14 denitrification pathway
154 between two strains, a NO producer and a NO consumer, to make a synthetic community that
155 could catalyze the complete denitrification reaction (Figure 2A). We reasoned that such a
156 community would allow an NO producing strain to supply a low but steady concentration of NO
157 to its partner consumer strain, minimizing toxicity issues and circumventing the need to work
158 with NO donor molecules. Because of the sequential nature of the denitrification steps, we
159 began by creating and characterizing several single, double, triple and quadruple clean deletion
160 mutants to split the first and second half of the pathway at NO between two strains (Figure S1).
161 After several iterations, we settled on a co-culture consisting of two strains that allowed us to
162 observe NO cross-feeding via the presence or absence of growth under anoxic conditions
163 (Figure 2A, co-culture 4 from Figure S1A). The NO producer strain, magenta outline, lacks both
164 the NO reductase (Nor) as well as the N_2O reductase (Nos). Compared to WT (black) under
165 anoxic growth with nitrate (Figure 2B), the producer strain shows a dramatic defect in growth.
166 This is consistent with previously characterized Nor mutants that can accumulate upwards of 15
167 μM NO before triggering a negative feedback loop that represses further nitrate and nitrite
168 reduction, preventing further NO production [16]. To ensure NO would be the sole TEA available

169 for use, we designed the NO consumer strain to lack both the nitrate reductases (the proton
170 pumping, membrane bound Nar and the redox balancing, periplasmic Nap), and nitrite
171 reductase. Compared to WT, the consumer strain (cyan) also shows a dramatic growth defect,
172 but unlike the producer strain, without NO inhibition, shows slight growth likely due to small
173 amounts of carryover oxygen or built-up energy stores from the inoculum (Figure 2B). When
174 these two strains are co-cultured to complete the pathway (dark blue), we see a large increase
175 in total growth, as would be expected if the producer were relieved of deleterious NO build-up,
176 and the consumer were provided with a low-level supply of an otherwise toxic TEA. (Figure 2B).
177 To verify that the growth of the strains in the anoxic co-culture was due to the removal of
178 NO from the producer by the consumer, we functionally replaced the consumer with the
179 chemical NO scavenger, c-PTIO, and grew the NO producer strain in its presence or absence.
180 Compared to growth without the addition of c-PTIO restored NO producer growth, supporting
181 the interpretation that NO reduction by the consumer drives growth in the co-culture (Figure 2C).
182 Further, to address whether the consumer's reduction of NO in the co-culture caused it to grow,
183 we removed the NO reductase (Nor) from the consumer strain (Figure S1C). While this deletion
184 did not alter the growth of this strain alone (Figure S1C, cyan), co-culturing this strain with the
185 NO producer not only prevented, but also appeared to hinder co-culture growth completely
186 (Figure S1C, dark blue). Finally, we asked if substrate level phosphorylation via pyruvate
187 fermentation, a means of ATP generation for long term anaerobic survival in PA [35], might
188 contribute to consumer growth by using NO in a redox balancing role as occurs for phenazines,
189 another redox-active metabolite made by PA [36]. As with Nor deletion, removal of genes
190 responsible for substrate level phosphorylation (*ackA* and *pta*) did not have a measurable effect
191 on maximum OD reached using a plate reader (Figure S1D, cyan). However, unlike Nor
192 removal, the co-culture's maximum OD was unaffected by the consumer's ability to perform this
193 process (Figure S1D, dark blue), suggesting consumer growth may be attributed to energy
194 conservation from NO reduction as graphically depicted in Figure 1B.
195 These experiments suggest there is a net community benefit to strains in planktonic co-
196 culture with a partitioned denitrification pathway under anoxic conditions compared to
197 monoculture. To unpack this bulk phenotype and discern the effects of co-culture on the two
198 members, we co-cultured the NO producer and consumer expressing constitutive fluorescence
199 markers (GFP or mApple) for 48 hours. To track each strain's growth in the mixed population,
200 we performed serial dilutions of the anoxic culture and plated for CFUs under oxic conditions.
201 Using a fluorescence microscope and image analysis, we calculated the change in starting cell
202 numbers and ratio of the two strains at the final time point (Figure 2D). Alone, the NO producer,

203 regardless of the fluorescence reporter used, showed no change in CFU after 48 hours (Figure
204 2D). This indicates NO production under these conditions reached inhibiting levels, but not
205 necessarily enough to cause death. The NO consumer in the absence of the producer exhibited
206 slight growth (Figure 2D), as seen in the growth curves (Figure 2B). Finally, we measured the
207 growth dynamics of each strain in the co-culture. Regardless of the starting ratio (more
208 producer, more consumer, or equal) both strains grew significantly, converging on an even ratio
209 of producer to consumer by 48 hours (Figure 2D). These results demonstrate that NO, when
210 supplied at a low but steady level, can serve as a TEA to support slow anoxic growth. This
211 exchange promotes a mutualistic interaction where growth inhibition of the producer is alleviated
212 by the consumer, which in turn gains a TEA; together, they flourish.
213
214 **NO cross-feeding under anoxic and sessile conditions is mutually beneficial and**
215 **proximity dependent.**
216 Next, we wondered how spatial structure might influence the growth of the producer and
217 consumer given that NO is a highly reactive and diffusible molecule. We hypothesized that,
218 unlike under shaken planktonic growth conditions in which the whole population benefits, under
219 spatially constrained anoxic conditions, proximity determines the success of community
220 members. To test this prediction, we mixed fluorescently labeled cells of the same or differing
221 genotypes in equal ratios, diluted the cultures, and sandwiched them between a coverslip and a
222 nitrate-supplemented agar medium pad such that single cells were randomly distributed from
223 one to dozens of cell lengths from each other. From these starting points, single cells could
224 develop into aggregate biofilms over a 48-hour period. Figure 3A graphically represents the
225 strain mixtures shown in Figure 3B as well as their predicted interactions based on the results of
226 our planktonic growth experiments. As controls, we mixed WT with WT to explore how two cells
227 with the full pathway and no growth defects would interact under these conditions, as well as the
228 consumer and producer strains with themselves. Finally, the producer and consumer strains
229 were mixed to visualize their interaction.
230 Using widefield microscopy, we observed the two strains (GFP/mApple) in the WT
231 mixture grew as large clonal expansions with little single cell intermixing, indicating neither was
232 impacted by the other (Figure 3B-3C) [37,38]. In contrast, both the Pro+Pro and Con+Con mixtures
233 showed a dramatic reduction in aggregate size (proxy for total growth accumulation until
234 observation, 48 hours) compared to WT (Figure 3B), in line with the inability of these strains to
235 reduce nitrate, the supplied TEA. Interestingly, in order to observe this low baseline of growth
236 for the consumer strain when grown with itself, it was necessary to use a consumer strain

237 deficient in pyruvate fermentation. Whereas optical density was unable to resolve a difference
238 between consumer strains +/- fermentation capability, this single cell imaging approach
239 significantly increased our growth detection sensitivity, enabling measurement of subtle, but
240 significant, differences (Figure S2A-2C, compare with Figure S1D, cyan). If we compare the WT
241 (Figure 3C) and co-culture (Figure 3D) under these conditions, most strikingly we observe an
242 increase in single cell intermixing between the two strains for the co-culture (Figure 3B vs 3D).
243 The two WT strains (GFP/mApple) appear to grow as clonal expansions, pushing against one
244 another rather than maximizing cell-cell contact (Figure 3C). Conversely, the co-culture shows
245 slower growth compared to WT (same under planktonic growth), but appears to favor cell-cell
246 contact between strains, forming mixed aggregates (Figure 3D), suggestive of a reliance of
247 each partner on one another for continued growth [39]. These mixed aggregates likely resulted
248 from close starting positions of producer and consumer cells.
249 In addition to intermixed co-culture aggregates, we also observed a difference in
250 aggregate size between single genotype mixtures and the co-culture (Figure 3E). If we compare
251 producer aggregates (Pro+Pro, GFP or mApple dots) to the producer aggregates when grown
252 with the consumer strain (Pro+Con, mApple dots) we see a significant increase in aggregate
253 size (Figure S2D); thus, even when the producer is not in direct contact with the consumer, it
254 appears to benefit from NO removal at distance. The consumer strain (Con+Con, GFP or
255 mApple dots) also showed a small but statistically significant increase in size even when not in
256 direct contact with the producer (Pro+Con, Cyan dots) (Figure S2D). However, the largest
257 aggregates were those that contained a mixed population of producer and consumer strains
258 (blue dots) (Figure 3E and Figure S2D).
259 Importantly, the increase in aggregate size even when the co-culture strains where not in
260 direct contact indicates that while single cell intermixing can occur when the two strains are
261 seeded at close initial starting positions (Figure 3D), without a proximal sink, NO can diffuse
262 outward from producer cells to reach consumer cells thereby increasing the interaction range.
263 NO's ability to rapidly traverse the distances separating source from sink cells in our mixed
264 cultures is not surprising given prior results showing that NO can diffuse over 100 μm within 1
265 second [40]. To determine whether diffusion alone could explain our results, we measured the
266 Euclidean distance between the centers of each aggregate at 48 hours in producer-alone,
267 consumer-alone and co-cultures. When we compare the minimum distance between each
268 aggregate and its closest neighbor, we find that all are within 100 μm of each other, with the
269 majority between 20-60 μm (Figure 3F). Notably, there is a slight decrease in distances between
270 co-cultured aggregates, likely due to better growth given the exchange of NO. Together, these

271 results extend our planktonic growth observations into a spatial context, revealing how
272 community members with a partitioned denitrification pathway can interact under anoxic
273 conditions where NO can freely diffuse.
274
275 **Oxygen availability enhances NO toxicity, thereby changing the nature of the co-culture**
276 **interaction.**
277 Recognizing that oxygen presence increases NO toxicity (Figure 1B) and that many
278 environments where denitrification occurs experience dynamic changes in oxygen and nitrate
279 consumption coupled to increased production of nitric and nitrous oxide [5,41], we wondered what
280 would happen to the NO producer strain and co-culture when grown in a heterogeneously
281 oxygenated environment. Strains such as PA14 are facultative anaerobes, meaning they
282 preferentially respire oxygen when it is available (oxic conditions), but when oxygen is limited,
283 they induce pathways (such as denitrification) that permit energy conservation using alternative
284 TEAs. A classic example of this phenomenon is when cells grow planktonically but are not
285 shaken during growth. Cells at the surface of the medium reduce oxygen faster than it can
286 diffuse into the culture, resulting in an oxygen gradient (Figure 4A, left) [42]. To expand our
287 understanding of when, where and how NO-cross feeding operates, we exploited this
288 phenomenon and measured growth in shaking or standing "oxic" cultures. We hypothesized that
289 strains harboring a partitioned denitrification pathway would exhibit growth that depends on the
290 amount of oxygen and nitrate present, in a manner reflecting the agathokakological effects of
291 oxygen and NO on cells.
292 To test this hypothesis, we first observed how stagnantly grown cultures created an
293 oxygen gradient by measuring the oxycline of both the WT and co-culture at multiple time points
294 using an oxygen microelectrode (Figure 4B). The oxycline was present and consistent between
295 strains and time points. As a baseline, we tracked the growth of the producer and consumer
296 strains, alone and in co-culture, over 48-hours in a continuously shaking plate reader to prevent
297 an oxygen gradient from forming. In the absence of nitrate all strains grew similarly, as
298 expected, indicating the genetic modifications had no off-target effects (Figure 4C). Conversely,
299 with 5 mM nitrate added to the medium, the consumer showed a slight growth defect compared
300 to the WT and the producer displayed a brief growth arrest midway through exponential phase,
301 with growth then paralleling that seen for the WT or mixed producer + consumer cultures
302 (Figure 4D). Despite continuous shaking, at these cell densities, we surmise from prior work that
303 these strains began to experience oxygen-limitation during mid exponential phase [42].

304 To further induce hypoxia, we performed the same planktonic growth experiment without
305 the plate reader shaking, mimicking the conditions leading to the oxycline shown in Figure 4B.
306 Again, in the absence of nitrate, we did not see a difference between the strains (Figure 4E).
307 However, in the presence of nitrate, all but WT showed a slight lag in growth (Figure 4F).
308 Importantly, even without the ability to reduce nitrate, the consumer was able to eventually
309 reach the same final OD as WT. Conversely, the producer strain showed a dramatic decrease in
310 OD later in the growth curve, suggestive of cell lysis. To check whether this reduction in OD was
311 due to a reduction in viable cells, we counted CFUs. Compared to WT viability at the 48hr time
312 point, there was a significant reduction in producer CFU (Figure S3A). To confirm whether
313 growth and prevention of cell death in the co-culture was caused by NO consumption, we
314 repeated the growth curve but this time with a consumer strain lacking the NO reductase (Nor)
315 (Figure S3B). When the Nor deficient consumer strain was co-cultured with the producer under
316 hypoxic conditions, we observed a reduction in OD similar in timing and amount to the producer
317 growth alone. Because the consumer alone reaches the same final OD as WT, yet would
318 otherwise die if it lacked NO reduction ability in the co-culture, we propose that under hyp(oxic)
319 conditions the consumer plays a beneficial role in the mixed community
320 Finally, to assess whether concomitant aerobic respiration and denitrification were
321 occurring under these conditions, we tracked the accumulation of superoxide (O_2^-) and NO. O_2^-
322 is a by-product and intermediate of oxygen respiration that is typically removed by superoxide
323 dismutase (SOD) (Figure 4A, right). However, NO readily reacts with superoxide (O_2^-) to form
324 the reactive nitrogen species, peroxynitrite ($ONOO^-$), which can out-compete superoxide for
325 SOD leading to an accumulation of reactive oxygen species and lead to oxidative stress (Figure
326 4A, right) [17]. Thus, we reasoned that the increase in cell death observed under hypoxic
327 conditions for the NO producer might correlate with an inability to scavenge superoxide. To test
328 this idea, we used a O_2^- sensitive dye (CellROX, Figure 4G) and an intracellular NO sensitive
329 dye (DAF-2DA, Figure 4H) to detect their production. Both O_2^- and NO increased over the
330 growth curve in the producer strain when grown alone (Figure 4G-4H), with a rise in signal
331 around 30 hours, correlating with the drop in OD (Figure 4F, arrows). This decrease in OD and
332 increase in O_2^- signal likely occurs due to cell death and thus a collapse of the oxygen gradient
333 leading to a cascade of further ROS production.
334
335 **NO cross-feeding under (hyp)oxic and sessile conditions leads to spatial behavioral**
336 **patterns.**

337 Unlike under anoxic conditions where the consumer strain gains a TEA that allows it to
338 grow, we wondered what role its reduction of NO would play under heterogeneously
339 oxygenated, sessile growth conditions. To achieve this, we grew diluted cells on agar pads
340 under oxic conditions into aggregate biofilms (Figure 5A). Unlike the anoxic experiments, here
341 cells initially had full access to oxygen and thus we expected them to behave as in planktonic
342 oxic growth conditions. Over time, we expected cell density to rise and oxygen to diminish,
343 prompting greater nitrate reduction to NO by the producer strain, as seen under planktonic
344 hypoxic growth conditions. The question became: how would the fixed organization of NO
345 producers and consumers in space influence their behavior over time?
346 To visualize interactions between NO producers and consumers, we mixed the strains
347 with themselves or each other and incubated them under oxic conditions on nutrient agar pads
348 containing nitrate. After 24 hours of growth, we observed with widefield fluorescence
349 microscopy that WT, like under anoxic conditions, grew into aggregate biofilms; however, rather
350 than monolayers, these biofilms appeared thicker perhaps due to their access to oxygen and
351 ability to support both oxic and anoxic populations (Figure 5B). Strikingly, the producer only
352 mixture (Pro+Pro) also showed clonal patches (outlined with a dotted white line, Figure 5B) but
353 with very few cells remaining fluorescent. To investigate further, we examined fluorescence and
354 corresponding phase channels more closely (Figure S3C-3E). Cells that maintained their
355 fluorescence after this incubation period also maintained their opacity in the phase channel.
356 Cells no-longer showing fluorescence appeared transparent, leading us to conclude that they
357 have undergone cell death and lysis as seen under hypoxic planktonic growth (Figure 4F).
358 Conversely, the consumer only mixture (Con+Con) grew into clonal patches, (note much larger
359 than under anoxic conditions due access to oxygen as a TEA) though they did not appear as
360 dense as WT owing to their inability to support anoxic growth with nitrate.
361 The co-culture, however, provided several new insights. First, there was an increase in
362 single cell intermixing (compare Figure 5C (no mixing) and 5D (mixing)). Second, unlike under
363 planktonic growth conditions where the whole co-culture population benefits from interacting,
364 here there appeared to still be lysis of producer cells when not in proximity to consumer cells
365 (Figure 5D, Figure S4A shows lysis overtime). This indicates that spatiotemporal,
366 microenvironmental changes induce metabolic dynamics that unlock a spatial niche where
367 cross-feeding provides a selective advantage as protection from lysis for the producer strain.
368 Such protection spatially patterns in several ways (Figure 5E): producer cells follow the
369 consumer contour; others appear to be protected by a pocket formed by consumer cells; and
370 still others are protected in regions of high intermixing. Knowing that the producer cells would

371 lyse without local NO depletion under hypoxic conditions (Figure 4F) permits us to link such
372 cellular spatial arrangement to physiological activity.
373
374 **NO-dependent, co-culture interaction patterns dynamically reflect changes in the**
375 **microenvironment**
376 To test our predictions about how these spatial patterns arise, we repeated agar pad
377 imaging as in Figure 5, but varied whether or not the consumer strain encoded the nitric oxide
378 reductase (Nor). First, we asked whether the presence of Nor decrease ROS stress by
379 preventing the downstream generation of superoxide. To address this, we included CellROX in
380 the agar from the beginning of the experiment to visualize super oxide accumulation using
381 confocal microscopy (Figure 6A-6D). The consumer channel was used to generate a mask and
382 measure CellROX fluorescence intensity of the consumer only space (illustrated in Figure S4B).
383 Comparing the results of consumer strains with (Figure 6A) and without (Figure 6B) Nor, we
384 found a dramatic increase in CellROX staining at the border between the strains, and a
385 measurable increase in the consumer cells surrounding the producer cells. This suggests NO
386 diffusion leads to ROS generation in the absence of NO reduction by the consumer. Next, we
387 asked how the consumer affects the producer cells in these biofilms by measuring the
388 remaining producer cell area as a function of available, non-consumer space (inverse of
389 consumer mask, illustrated in Figure S4B). The results show a dramatic reduction in producer
390 area when the consumer lacks the ability to reduce NO (Figure 6D).
391 Finally, these end time point measurements assumed where the border between
392 consumer and producer started. The increase of CellROX staining at the border when the
393 consumer lacked NO reductase suggests it could be undergoing lysis itself. This led us to ask if
394 the consumer lysis when NO cannot be reduced matches the protection afforded to the
395 producer when it can be reduced. We performed time lapse microscopy of the two co-cultures
396 (consumer +/- Nor) both pre- and post-lysis. This allowed us to mark the initial border (Figure
397 6E, solid line) between the strains and draw a line indicating the extent of protection (Con + Nor)
398 or induction (Con - Nor) of lysis (Figure 6E, dashed line). Indeed, the consumer strains without
399 Nor undergo lysis at the border with the producer (Figure 6F), suggesting the major role for its
400 NO reduction under these conditions is first to protect itself from toxicity, with a secondary
401 benefit for the producer. Quantifying this phenomenon, we measured the range of protection
402 (distance) conferred to the producer by the consumer (arrows, Figure 6E; pink line-Figure 6G).
403 When the consumer lacks NO reduction capacity, all of the producer is vulnerable to lysis and
404 the equivalent protection range manifests as a lysis range in the consumer population due to

405 NO diffusion (Figure 6F, cyan line-Figure 6G). Overall, these ranges (2-12 μm) are much shorter
406 than the interaction distances observed under anoxic growth conditions (20-60 μm, Figure 3F).
407 We interpret this to be a consequence of NO's high reactivity with oxygen effectively shortening
408 its diffusive range. Figure 6H graphically depicts our working model, showing how initially non-
409 interacting cells can develop a high stakes interaction with respect to fitness as the
410 microenvironment changes.
411
412 **Discussion**
413 Awareness of the diversity of microbial metabolic interactions is expanding with
414 improved techniques for identifying new pathways and observing interactions [1,43–47]. In the face
415 of this progress, gaining a better understanding of how these interactions may shift as a function
416 of dynamic oxygen gradients is an important goal. We developed a synthetic microbial
417 community linked by the exchange of NO, a redox active molecule whose biological effects are
418 tuned by the presence of oxygen, as a step towards this end. Our work shows that the
419 interactions that drive NO intercellular exchange and reduction are induced and sensitive to the
420 genetic content of community members and microenvironmental gradients, knowledge of which
421 leads to predictable organizational outcomes.
422 Given denitrification may be a community effort [23], and that each community member
423 may contain a different suite of relevant enzymes, our studies with a synthetic community
424 suggest that certain agathokakological intermediates, such as NO, may play an outsized role in
425 structuring natural microbial communities. Linking environmentally-dependent metabolic
426 interactions to microscale microbial organization is an important goal [48–53]. Our findings spotlight
427 dynamic changes in local oxygen for its ability to tune both the nature and need for a cross-
428 feeding relationship. In our example case, NO can generate toxic byproducts under oxic
429 conditions, leading to cellular growth arrest. Yet under anoxic conditions, NO can be a lifeline,
430 serving as a TEA and promoting energy conservation and growth. These contrasting effects are
431 important because oxygen exhibits steep environmental gradients over small spatial scales [5,54].
432 Our work draws attention to the fact that oxygen gradients can shape microbial interactions both
433 in planktonic and sessile communities, with the scales over which these interactions occur being
434 set by the proximity of interacting cells and their local microenvironment, which they in turn alter
435 in space and time.
436 An important next step will be to determine whether mixtures of natural isolates with
437 partitioned metabolic pathways play by the same rules. Our work gives rise to testable
438 predictions about when and where NO cross-feeding may occur. For example, it is well

439 appreciated that NO is an important intermediate species in the nitrogen cycle [22], whose
440 turnover rates may decide the fate of soil nitrogen stores. Interestingly, recent metagenomic
441 studies indicate that within certain habitats, there an enrichment for organisms that can only
442 reduce NO to N_2O, an important greenhouse gas [45]. Thus, an understanding of what constrains
443 NO reduction may provide insight into a metabolic process with important environmental
444 consequences. Recent studies have drawn attention to the potential for partitioned pathways to
445 influence the rate of nitrogen flux in soils by resident microbes [23,45]. Our work attempts to directly
446 link structure and function of such partitions as is suggested by the genomic content of
447 environmental isolates [45]. In an entirely different context, our finding that *P. aeruginosa* can
448 thrive by reducing NO provided by another cell lends credence to the hypothesis that PA may
449 survive the host immune NO attack by its reduction to N_2O, and may correlate with the
450 appearance of N_2O in the breath gas of cystic fibrosis patients [54]. Importantly, *P. aeruginosa* can
451 be found proximal to host immune cells in these infected environments [44].
452 Finally, we note that NO is only one of many redox active molecules (RAMs), both
453 organic and inorganic, that may help structure microbial communities over small spatial scales
454 as a function of oxygen availability. For example, other RAMs such as phenazines can function
455 as natural toxins or beneficial agents of nutrient acquisition and/or redox homeostasis,
456 depending on the context [9]. Similarly, sulfide has long been known to play nuanced roles in
457 nature, with its concentration-dependent toxicity influencing which phototrophic species are able
458 to thrive [55] and where different energy-conserving processes can occur within microbial mats
459 [56,57]. Many other parameters may be subject to similar dynamic spatiotemporal gradients, such
460 as carbon, pH and light, and are likely to also play important roles in determining the niches
461 where cross-feeding or other types of metabolic interactions can occur ([29,30,58]). Towards the
462 goal of gaining a predictive understanding of why diverse microbial communities are structured
463 the way they are, a constructive next step will be to model these interactions in light of
464 fluctuating environmental parameters, iterating with experiments until cross-cutting principles
465 can be identified with predictive power.
466
467 **Acknowledgments.** The work was supported by the National Institutes of Health
468 (R01HL152190 to D.K.N.) and the National Science Foundation Graduate Student Fellowships
469 Program (to S.A.W.). We would like to thank the current and past Newman Lab members for
470 feedback and discussions. Specifically, we thank Drs. Darcy McRose and Avi Flamholz for
471 manuscript review, Dr. Melanie Spero for molecular technique instruction, Drs. Reinaldo Alcade,
472 Georgia Squyres, and Zachary Lonergan for fruitful discussion and assay troubleshooting, and

Dr. Michael Piacentino for help with programming and encouragement. Some of the imaging was performed in the Biological Imaging Facility of the California Institute of Technology, with the support of the Caltech Beckman Institute and the Arnold and Mabel Beckman Foundation.

Author contributions.

SAW and DKN contributed to study conceptualization, data interpretation and writing – review and editing. SAW developed methodology, performed experiments, data curation, and original manuscript draft.

Inclusion and diversity.

One or more of the authors of this paper self-identifies as a member of the LGBTQIA+ community. We support inclusive, diverse, and equitable conduct of research.

Declaration interests. DKN is a member of the Current Biology Editorial Board.

Main-text figure legends.

Figure 1. The agathokakological roles of nitric oxide in *Pseudomonas aeruginosa* growth. (**A**) WT PA14 sequentially reduces nitrate to nitrogen gas using five major enzymes. (**B**) Proposed mechanism of energy conservation using NO as the sole starting terminal electron acceptor (TEA). (**C**) WT PA14 survival after exposer to a short burst of an NO donor molecule under anoxic or oxic conditions. P value from unpaired t-test. Each dot represents one replicate, n=6 per condition.

Figure 2. Design and characterization of synthetic nitric oxide cross-feeding community. (**A**) Schematic of NO producer (magenta) and consumer (cyan). Genes that have been cleanly deleted are grayed-out, and those remaining are shown in black. The pathway partitions where NO is produced and reduced. (**B**) Growth curve of strains in (A) grown individually and in co-culture (partitioned pathway), compared to WT (full pathway), over 72hrs under anoxic conditions with 5mM nitrate as sole provided terminal electron acceptor (TEA). Each growth curve represents n=4 replicates. (**C**) Growth rescue of producer strain using the chemical NO scavenger c-PTIO. Line and error bars represent means and standard deviations; P value from unpaired t-test. Each dot represents one replicate, n=3 per condition. (**D**) Different mixtures of the producer and consumer strains constitutively expressing either a GFP or mApple fluorescence reporter were grown as in (B) but at the beginning and end of a 48 hour incubation

507 were plated for colony forming units. Consumer strain is Δ*narGHJI*Δ*nirS*Δ*napAB*Δ*ackApta*.
508 Producer strain is Δ*norCB*Δ*nosZ*. See also Figure S1 and Table S1. Each dot represents one
509 replicate, n=3 per condition
510
511 **Figure 3. Patterning of producer and consumer strains under sessile anoxic conditions.** (**A**)
512 Phenotypic predictions. (**B**) Representative images showing growth patterns of indicated strain mixtures
513 constitutively expressing either GFP or mApple after anoxic growth for 48hrs under an agar pad with
514 nitrate provided as sole TEA. (**C,D**) Zoom-in of WT mixture showing strains growing as clonal patches
515 (C) compared with zoom-in of the co-culture showing intermixing (D). (**E**) Quantification of each
516 aggregates (dots) size and color-coded based on whether the aggregate contained just GFP, mApple
517 or both (mixed) cells. (**F**) ECDF plot of the Euclidean distance between each aggregate and its closest
518 neighboring aggregate. Consumer strain is Δ*narGHJI*Δ*nirS*Δ*napAB*Δ*ackApta*. Producer strain is
519 Δ*norCB*Δ*nosZ*. E and F display values from at least 190 aggregates measured from at least 25 images
520 per condition, pooled from two independent replicates. See also Figure S2.
521
522 **Figure 4. Oxic vs hypoxic growth of planktonic cultures supplemented with and without nitrate.**
523 (**A**) Graphical prediction of the heterogeneously oxygenated environment created by stagnate liquid
524 culture incubation (left). Expected consequences of the NO producer growing under this environment
525 (right). Superoxide (O_2^-) produced during aerobic respiration is kept below toxic levels by superoxide
526 dismutase (SOD). The byproduct of NO and O_2^-, $ONOO^-$, can out-compete O_2^- for SOD causing an
527 accumulation of O_2^- (**B**) Oxygen profiles from non-shaking cultures of the WT compared to profiles from
528 the co-culture at two time points to confirm heterogeneity. Each trace represents n=3 replicates. (**C-F**)
529 48hr growth curves cultured under the indicated conditions. Evenly oxygenated environments ("oxic-
530 shaking") were achieved by shaking cultures during incubation (C,D), while unevenly oxygenated
531 environments ("hypoxic-stagnant") were achieved by culturing without shaking (E,F). (**G-H**) Fluorescent
532 dye readings of superoxide (G) and nitric oxide (H) accumulation over a hypoxic growth curve with
533 nitrate (as in F). Consumer strain is Δ*narGHJI*Δ*nirS*Δ*napAB*. Producer strain is Δ*norCB*Δ*nosZ*. Each
534 trace in C-H represents n=3 replicates. See also Figure S3.
535
536 **Figure 5. Patterning of producer and consumer strains under sessile oxic conditions.** (**A**)
537 Graphical prediction for NO producer and consumer strains growing initially in the presence of replete
538 oxygen. Overtime oxygen consumption will lead to hypoxia and presumably a higher and higher
539 production of NO. (**B**) Representative images of indicated strains grown as biofilms for 24hrs under oxic
540 conditions in the presence of nitrate. (**C**) Zoom-in of WT clonal expansion showing no intermixing. (**D**)

541 Zoom-in showing producer survival adjacent to the consumer expansion interface; note that cells
542 appear brightest prior to lysis. (**E**) Three additional high magnification callouts to spotlight specific
543 structural features. Consumer strain is Δ*narGHJI*Δ*nirS*Δ*napAB*. Producer strain is Δ*norCB*Δ*nosZ*. See
544 also Figures S3 and S4.
545
546 **Figure 6. Dynamic spatial patterning of NO partitioned community.** (**A-D**) Visualization and
547 quantification of spatial superoxide production and lysis as a function of NO consumers presence
548 (+Nor) or absence (-Nor) of the NO reductase. Specified strains were grown as in Figure 5 but including
549 the superoxide sensitive dye CellROX (Yellow). (**C**) Mean CellROX intensity of consumer cells was
550 measured whether it contained the NO reductase (A) or not (B). (**D**) Using the inverse of the consumer
551 region as a pre-lysis producer area mask compared to the remaining producer area (unlysed), a %
552 remaining metric was obtained. P values from unpaired t-tests in C and D. Each dot represents
553 measurements from single images ($n \geq 10$). (**E-F**) To measure lysis range in the presence or absence of
554 NO reductase, time lapse imaging was performed from pre- and post-lysis. (**G**) ECDF of lysis/protection
555 from lysis range was measured from 12 regions each from three aggregate co-culture interfaces
556 (between solid and dashed lines as drawn in E and F, n=36). (**H**) Proposed model in which the NO
557 producer and consumer strains both grow clonally until the microenvironment changes such that the
558 producer begins to produce NO and lyse. The consumer acts as a sink for NO in close proximity to the
559 producer, relieving NO toxicity and preventing the producers and own lysis. Consumer strain is
560 Δ*narGHJI*Δ*nirS*Δ*napAB*. Producer strain is Δ*norCB*Δ*nosZ*. See also Figure S4.
561
562

563 **STAR Methods.**

564 **KEY RESOURCES TABLE**

565 See attached table

566

567 **RESOURCE AVAILABILITY**

568 **Lead Contact**

569 The lead contact of this study is Dianne Newman (dkn@caltech.edu) who will fulfill all requests
570 for additional information, resources, and reagents.

571

572 **Materials availability**

573 Bacterial strains and constructs that were generated in this study are available upon request to
574 the lead contact.

575

576 **Data and code availability**

577 This paper does not report original code. All source images, raw data, and any other information
578 necessary to replicate these analyses will be shared by the lead contact upon request.

579

580 **EXPERIMENTAL MODEL AND SUBJECT DETAILS**

581 **Bacterial strains**

582 All strains used are clean deletion mutants originating from the wild-type (WT)
583 *Pseudomonas aeruginosa* UCBPP-PA14 strain as described below in the Method Details.
584 Strains were stored as 50% glycerol stocks at -80°C.

585

586 **Bacterial growth conditions**

587 Before use, strains were streaked from frozen stock onto Bacto agar (BD, Sigma) plates
588 containing LB (Miller, BD, Sigma) or LB supplemented with 50 µg/mL gentamicin (GoldBio) to
589 select for retention of expression cassettes within fluorescent strains, and grown overnight at
590 37°C. From streak plates, a dab of culture was used to inoculate 5 mL liquid cultures in LB or LB
591 plus 50 µg/mL gentamicin liquid media. Cultures were shaken at 250 RPM at 37°C overnight
592 until fully saturated at stationary phase. To standardize inoculum sizes between strains, each
593 strain's optical density (OD_{500nm}) was measured by spectrophotometry (Beckman Coulter).
594 Strains were then each washed and diluted to an OD of 1 via centrifugation and resuspension in
595 phosphate buffered saline (PBS). Strains were then either further diluted directly, or first mixed
596 at equal ratios for co-culture experiments and then diluted to final experimental concentrations.

597 For all experiments, a Low Salt LB (LSLB) was used instead of standard LB powder due to
598 microelectrode reactivity to the high NaCl concentration. The composition of LSLB was 141 mM
599 Tryptone (BD, Sigma), 16mM Yeast Extract (BD, Sigma), 45mM NaCl (Fisher Chemical), which
600 were dissolved in Mili-Q water and autoclaved. Nitrate was supplemented into media where
601 indicated by diluting from a 1M stock of KNO_3 (Fisher Chemical).
602
603 **METHOD DETAILS**
604 **Construction of mutant bacterial strains**
605 Table S1 contains a full list of primers used in the creation of deletion constructs and
606 mutant strains used in this study. Briefly, a 1kb fragment up- and downstream of the target gene
607 was amplified via PCR and cloned into the pMQ30[59] plasmid using Gibson cloning (NEB) and
608 transformed into *E. coli* cells as previously described [60]. Deletion constructs were then
609 introduced to parent strains (WT PA14 and or deletion strains of PA14, see Table S1) via
610 triparental conjugation. *E. coli* plasmid and helper strains were selected against by bead plating
611 on VBMM plates containing 50 µg/mL gentamicin [61]. Roughly 50% WT and 50% clean deletion
612 colonies were then obtained by bead plated on a 10% sucrose plate to induce homologous
613 recombination with the construct containing the regions up- and downstream, but lacking the
614 targeted gene locus [62]. Clean deletion strains were confirmed via PCR genotyping using primers
615 that span the deletion region and sequencing of the amplified product. Finally, anaerobic growth
616 challenges revealed expected physiological effects (e.g. ΔnirS was unable to grow on nitrite,
617 etc). Fluorescence strains were created as previously described using plasmids driving
618 GFP/mApple expression under control of the constitutive ribosomal promoter rpsG introduced
619 into the Tn7 site of specified strains using tetra-parental conjugation[62,63]. *E. coli* helper strains
620 were again selected against using VBMM containing 50 µg/mL gentamicin. Confirmation of
621 insertion was performed via microscopy, visualizing colonies in both green and red fluorescence
622 channels, and selecting those that were bright in their respective channel above background
623 autofluorescence.
624
625 **Serial dilution and colony forming unit (CFU) counting**
626 Liquid cultures were plated for colony forming units and back calculated to assess
627 number of cells. Typically, 100 µL of culture was placed into the well of a 96 well plate (at least
628 three technical replicates were assessed). 20 µL of culture was then diluted seven times in
629 serial 1:10 dilutions in PBS. 10 µL of the dilutions were then plated on a LB agar plate using a
630 multichannel pipette. The plates were then slanted vertically and tapped to allow the 10 µL to

631 spread in a line. All dilution plates were incubated under normal atmospheric conditions, in an
632 incubator at set to 37°C for roughly 24 hours. After incubation, colony counting was performed
633 either manually or with an imaging and image analysis pipeline (when fluorescence imaging was
634 used, see below). Dilutions with 100-200 colonies were used to calculate colony form units
635 (CFU/mL) by multiplying this number by the dilution factor.
636
637 **Growth curves**
638 Anoxic growth curve media was placed in anaerobic chamber 72 hours prior to
639 experiment to allow time for oxygen to degas from media. 1 OD_{500nm} cultures were brought into
640 chamber and further diluted to 0.005 OD_{500nm} in anoxic media. Growth curves were performed
641 using a BioTek Synergy 4 plate reader stored in an anoxic chamber and set to 37°C with
642 shaking and measured OD_{500nm} every 10 minutes. Oxic (shaking) and Hypoxic (stationary)
643 growth curves were set up as above but under normal atmosphere. Oxic growth curves were
644 performed using a Tecan Spark 10M set to orbital shaking. Hypoxic growth curves were
645 performed using a Spectramax M3 (Molecular Devices) plate reader set to not shake. Each
646 condition was performed in technical triplicate or quadruplicate. Each well contained 200 µL of
647 culture with 40 µL of autoclaved mineral oil added to the top of each well to prevent evaporation
648 of 48-72-hour growth curves. Traces from growth curves were analyzed and presented by
649 plotting mean OD_{500nm} over time (dark center line) and 95% confidence intervals from technical
650 replicates (shaded area) using Seaborn[64] plotting packages in Python [65].
651
652 **Nitric oxide and superoxide quantification**
653 Levels of nitric oxide and superoxide were quantitated using fluorescent dyes during
654 hypoxic growth curves. NO was quantitated using 50 µM DAF-2DA (Calbiochem, Sigma) which
655 is internalized by cells where esterases free DAF-2DA to interact with NO producing a green
656 fluorescence signal [66]. Superoxide was quantitated using 5 µM CellROX Deep Red (Thermo),
657 which is non-fluorescent in a reduced state but exhibits a strong induction of fluorescence upon
658 oxidation with reactive oxygen species [67]. The Spectramax plate reader was configured to
659 measure green fluorescence (Ex. 488 nm, Em. 520 nm, DAF-2) and far-red fluorescence (Ex.
660 640 nm, Em. 665 nm, CellROX). For pad imaging assays, CellROX was supplemented to the
661 agar pads directly at a final concentration of 10 µM and imaged after significant biofilm growth
662 had occurred to reveal superoxide localization. DAF-2DA was also used to visualize NO;
663 however, due to weak single-cell signal and strong background autofluorescence in the green
664 channel, we were unable to visualize the signal convincingly.

665

666 **Oxygen profiling**

667 To confirm the presence of oxygen gradients in standing cultures, we employed a 25 µm
668 diameter oxygen microelectrode (Unisense), which was calibrated as previously described [60].
669 Briefly, LSLB media incubated at 37°C was used to calculate the high point O_2 concentration. A
670 zero-point calibration was obtained by dissolving 2 g Sodium Ascorbate in 100 mL 0.1 NaOH,
671 which scavenges O_2 from the medium. Using the Unisense Sensor Suite Software to save
672 calibration values and control a motorized micromanipulator for profiling, O_2 was measured from
673 the surface of hypoxically incubated planktonic cultures in 1 mL Eppendorf tubes. The surface
674 was set by eye and confirmed by a reduction in mV signal. O_2 was then measured over a 1 mm
675 distance below the surface at 50 µm intervals. Two measurements were taken at each position,
676 and three technical replicates were averaged and displayed as the mean value with 95%
677 confidence intervals (Figure 4B). Cultures were prepared as in growth curves but maintained as
678 1 mL volumes in tubes rather than aliquoting into 96-well plates. Mineral oil was not added due
679 to potential incompatibility with electrodes.

680

681 **Agar pad imaging assay**

682 We determined that 1 OD_{500nm} cultures diluted to a starting concentration of 0.001
683 OD_{500nm} was sufficient to obtain single cells randomly distributed under agar pads. Agar pads
684 were made by combining LSLB media with 2% w/v Noble Agar (BD, Sigma). Prior to use, the
685 agar was melted by microwaving. To make equally sized agar pads, 100 µL was pipetted into
686 each of several square molds (6-7 mm X 7 mm X 1.6 mm Depth ID, 25 mm X 75 mm, Grace Bio
687 Labs), placed between two glass microscope slides, and allowed to solidify at 4°C until use.
688 Anoxic pads were made 72 hours in advance and placed in an anaerobic chamber to degas. 5
689 µL of 0.001 OD_{500nm} dilution culture was added to the well of an 8-well LabTek dish (Thermo).
690 Agar pads were then placed on overtop. Dishes were incubated at 37°C for 24 hours (oxic) or
691 48 hours (anoxic) in a sealed container (6.7 oz, Systema). When additional humidity was added,
692 instead of distinct aggregate biofilms, cells appeared as under intermixed planktonic conditions;
693 thus, additional humidity was not added. Time lapse imaging was performed incubating pads as
694 described above, but just before lysis would occur (~18 hours), dishes were sealed with parafilm
695 and placed in the heated microscope incubation chamber for imaging. Anoxically-incubated
696 cells were not initially fluorescent due to the inability for fluorophores to fold in the absence of
697 oxygen. To overcome this, pads were placed at 4ºC without lids for one to two hours prior to
698 imaging resulting in sufficient signal recovery to differentiate GFP and mApple positive cells.

699

700 **Microscopy**

701 All imaging was performed either using a Nikon Ti2 widefield fluorescence microscope or
702 a Zeiss LSM800 microscope. End time point agar pad images were collected using the Nikon
703 with a Plan Fluor 100x/1.30 oil phase objective and time lapse images were collected using a
704 Plan Apo 40x/0.90 dry phase objective. GFP channels were collected using a 488 nm LED
705 excitation light source and emission was collected with a FITC filter. The mApple channel used
706 561 nm LED light source and emission was collected with a TRITC filter. For time lapse
707 imaging, an OKO Labs cage incubation unit was set to 37°C several hours before imaging to
708 equilibrate the microscope stand and used for the duration. Images were collected every 20
709 minutes from multiple stage positions. Time indicated in figures represents time since the pads
710 were inoculated. Both fluorescence CFU counting images from Figure 2D and the
711 CellROX/Producer mass quantification images from Figure 6A-6B were collected using the
712 Zeiss LSM800 confocal with an EC Plan-Neo Fluor 1.25x/0.03 and Plan-Apochromat 63x/1.4
713 lens, respectively.

714

715 **Image analysis**

716 All images were analyzed and prepared for display using FIJI [68]. Brightness and contrast
717 were adjusted on a per image basis in order to best display cell positions and identifications,
718 unless otherwise noted (e.g. CellROX intensity in biofilms imaged and displayed the same for
719 comparison of intensity (Figure 6A-6B)). For time lapse imaging, agar pad XY drift was
720 accounted for by performing an image registration in FIJI using the StackReg plugin with the
721 Rigid Body option. For CFU counting and aggregate biofilm size measurements, images were
722 segmented following a background subtraction, contrast enhancement, and median filter. The
723 processed fluorescence channels were segmented using the Auto Local Threshold function.
724 Segmented objects were counted using the Analyze Particles function with a size filter set to the
725 average size of the specified objects. The XY image position was recorded and used to find the
726 Euclidian distance between aggregate biofilms on a per-image basis. Empirical Cumulative
727 Distribution Function (ECDF) plots (Figure 3F and Figure 6G) display 95% confidence intervals
728 and were generated in Python using iqplot [69].

729 CellROX intensity was measured from a subset of the images in Figure 6A-6B by
730 generating an intensity-based threshold binary mask of the consumer space (GFP channel).
731 The producer space was then found by inverting the consumer space. Finally, the producer
732 remaining was found by thresholding the producer channel (mApple). By finding the difference

733 between the producer space and producer remaining, a percentage was calculated (Figure 6D,
734 Figure S4B). Finally, to assess the distance in which the producer was saved from or induced
735 consumer lysis, the intensity profile of a line was drawn between the two points and used to
736 mark start and end and recorded for several images.
737
738 **QUANTIFICATION AND STATISTICAL ANALYSIS**
739 Quantification and analyses are described in the Method Details. Briefly, experimental
740 values were compiled and explored in Python and results were plotted using either Seaborn,
741 iqplot, or exported and displayed in GraphPad Prism v9. Statistical tests were performed in
742 GraphPad Prism v9, and the relevant statistical test and sample size is described in the
743 appropriate figure legend.
744

745 **References**

746

747 1. Zuñiga, C., Zaramela, L., and Zengler, K. (2017). Elucidation of complexity and prediction
748 of interactions in microbial communities. Microb. Biotechnol. *10*, 1500–1522.
749 10.1111/1751-7915.12855.
750 2. Ratzke, C., Barrere, J., and Gore, J. (2020). Strength of species interactions determines
751 biodiversity and stability in microbial communities. Nat. Ecol. Evol. *4*, 376–383.
752 10.1038/s41559-020-1099-4.
753 3. Niehaus, L., Boland, I., Liu, M., Chen, K., Fu, D., Henckel, C., Chaung, K., Miranda, S.E.,
754 Dyckman, S., Crum, M., et al. (2019). Microbial coexistence through chemical-mediated
755 interactions. Nat. Commun. *10*. 10.1038/s41467-019-10062-x.
756 4. Goldford, J.E., Lu, N., Bajić, D., Estrela, S., Tikhonov, M., Sanchez-Gorostiaga, A.,
757 Segrè, D., Mehta, P., and Sanchez, A. (2018). Emergent simplicity in microbial
758 community assembly. Science (80-.). *361*, 469–474. 10.1126/science.aat1168.
759 5. Krichels, A., DeLucia, E.H., Sanford, R., Chee-Sanford, J., and Yang, W.H. (2019).
760 Historical soil drainage mediates the response of soil greenhouse gas emissions to
761 intense precipitation events. Biogeochemistry *142*, 425–442. 10.1007/s10533-019-
762 00544-x.
763 6. Stewart, P.S., Zhang, T., Xu, R., Pitts, B., Walters, M.C., Roe, F., Kikhney, J., and Moter,
764 A. (2016). Reaction-diffusion theory explains hypoxia and heterogeneous growth within
765 microbial biofilms associated with chronic infections. npj Biofilms Microbiomes *2*, 1–8.
766 10.1038/npjbiofilms.2016.12.
767 7. Lowery, N.V., and Ursell, T. (2019). Structured environments fundamentally alter
768 dynamics and stability of ecological communities. Proc. Natl. Acad. Sci. U. S. A. *116*,
769 379–388. 10.1073/pnas.1811887116.
770 8. Dal Co, A., Ackermann, M., and van Vliet, S. (2019). Metabolic activity affects response
771 of single cells to a nutrient switch in structured populations. bioRxiv. 10.1101/580563.
772 9. Dahlstrom, K.M., McRose, D.L., and Newman, D.K. (2020). Keystone metabolites of crop
773 rhizosphere microbiomes. Curr. Biol. *30*, R1131–R1137. 10.1016/j.cub.2020.08.005.
774 10. Toyofuku, M., and Yoon, S.-S. (2018). Nitric Oxide, an Old Molecule With Noble
775 Functions in Pseudomonas aeruginosa Biology. In Advances in Polymer Science, pp.
776 117–145. 10.1016/bs.ampbs.2018.01.005.
777 11. Koppenol, H., and Koppenol, H. (2021). Nitric oxide, superoxide, and peroxynitrite: the
778 good, the bad, and the ugly.

12. Zumft, W.G. (1997). Cell biology and molecular basis of denitrification. Microbiol. Mol. Biol. Rev. *61*, 533–616. 10.1128/mmbr.61.4.533-616.1997.
13. Arai, H. (2011). Regulation and Function of Versatile Aerobic and Anaerobic Respiratory Metabolism in Pseudomonas aeruginosa. Front. Microbiol. *2*, 103. 10.3389/fmicb.2011.00103.
14. Koskenkorva, T., Aro-Kärkkäinen, N., Bachmann, D., Arai, H., Frey, A.D., and Kallio, P.T. (2008). Transcriptional activity of Pseudomonas aeruginosa fhp promoter is dependent on two regulators in addition to FhpR. Arch. Microbiol. *189*, 385–396. 10.1007/s00203-007-0329-3.
15. Sasaki, Y., Oguchi, H., Kobayashi, T., Kusama, S., Sugiura, R., Moriya, K., Hirata, T., Yukioka, Y., Takaya, N., Yajima, S., et al. (2016). Nitrogen oxide cycle regulates nitric oxide levels and bacterial cell signaling. Sci. Rep. *6*, 1–11. 10.1038/srep22038.
16. Yoon, S.S., Karabulut, A.C., Lipscomb, J.D., Hennigan, R.F., Lymar, S. V., Groce, S.L., Herr, A.B., Howell, M.L., Kiley, P.J., Schurr, M.J., et al. (2007). Two-pronged survival strategy for the major cystic fibrosis pathogen, Pseudomonas aeruginosa, lacking the capacity to degrade nitric oxide during anaerobic respiration. EMBO J. *26*, 3662–3672. 10.1038/sj.emboj.7601787.
17. Brunelli, L., Crow, J.P., and Beckman, J.S. (1995). The comparative toxicity of nitric oxide and peroxynitrite to escherichia coli. Arch. Biochem. Biophys. *316*, 327–334. 10.1006/abbi.1995.1044.
18. Yu, K., Mitchell, C., Xing, Y., Magliozzo, R.S., Bloom, B.R., and Chan, J. (1999). Toxicity of nitrogen oxides and related oxidants on mycobacteria: M. tuberculosis is resistant to peroxynitrite anion. Tuber. Lung Dis. *79*, 191–198. 10.1054/tuld.1998.0203.
19. Fang, Y., Koba, K., Makabe, A., Takahashi, C., Zhu, W., Hayashi, T., Hokari, A.A., Urakawa, R., Bai, E., Houlton, B.Z., et al. (2015). Microbial denitrification dominates nitrate losses from forest ecosystems. Proc. Natl. Acad. Sci. U. S. A. *112*, 1470–1474. 10.1073/pnas.1416776112.
20. Krichels, A.H., and Yang, W.H. (2019). Dynamic Controls on Field-Scale Soil Nitrous Oxide Hot Spots and Hot Moments Across a Microtopographic Gradient. J. Geophys. Res. Biogeosciences *124*, 3618–3634. 10.1029/2019JG005224.
21. Tian, H., Yang, J., Xu, R., Lu, C., Canadell, J.G., Davidson, E.A., Jackson, R.B., Arneth, A., Chang, J., Ciais, P., et al. (2019). Global soil nitrous oxide emissions since the preindustrial era estimated by an ensemble of terrestrial biosphere models: Magnitude, attribution, and uncertainty. Glob. Chang. Biol. *25*, 640–659. 10.1111/gcb.14514.

813 22. Kuypers, M.M.M., Marchant, H.K., and Kartal, B. (2018). The microbial nitrogen-cycling
814 network. Nat. Rev. Microbiol. *16*, 263–276. 10.1038/nrmicro.2018.9.
815 23. Gowda, K., Ping, D., Mani, M., and Kuehn, S. (2022). Genomic structure predicts
816 metabolite dynamics in microbial communities. Cell *185*, 530-546.e25.
817 10.1016/j.cell.2021.12.036.
818 24. Lycus, P., Bøthun, K.L., Bergaust, L., Shapleigh, J.P., Bakken, L.R., and Frostegård, Å.
819 (2017). Phenotypic and genotypic richness of denitrifiers revealed by a novel isolation
820 strategy. ISME J. *11*, 2219–2232. 10.1038/ismej.2017.82.
821 25. Rich, J.J., Heichen, R.S., Bottomley, P.J., Cromack, K., and Myrold, D.D. (2003).
822 Community Composition and Functioning of Denitrifying Bacteria from Adjacent Meadow
823 and Forest Soils. Appl. Environ. Microbiol. *69*, 5974–5982. 10.1128/AEM.69.10.5974-
824 5982.2003.
825 26. Hester, E.R., Jetten, M.S.M., Welte, C.U., and Lücker, S. (2019). Metabolic overlap in
826 environmentally diverse microbial communities. Front. Genet. *10*, 1–10.
827 10.3389/fgene.2019.00989.
828 27. Lilja, E.E., and Johnson, D.R. (2016). Segregating metabolic processes into different
829 microbial cells accelerates the consumption of inhibitory substrates. ISME J. *10*, 1568–
830 1578. 10.1038/ismej.2015.243.
831 28. Borer, B., Ciccarese, D., Johnson, D., and Ori, D. (2020). Spatial organization in microbial
832 range expansion emerges from trophic dependencies and successful lineages Benedict.
833 Commun. Biol., 1–10. 10.1038/s42003-020-01409-y.
834 29. Goldschmidt, F., Caduff, L., and Johnson, D.R. (2021). Causes and consequences of
835 pattern diversification in a spatially self-organizing microbial community. ISME J. *15*,
836 2415–2426. 10.1038/s41396-021-00942-w.
837 30. Goldschmidt, F., Regoes, R.R., and Johnson, D.R. (2018). Metabolite toxicity slows local
838 diversity loss during expansion of a microbial cross-feeding community. ISME J. *12*, 136–
839 144. 10.1038/ismej.2017.147.
840 31. Carr, G.J., Page, M.D., and Ferguson, S.J. (1989). The energy-conserving nitric-oxide-
841 reductase system in Paracoccus denitrificans Distinction from the nitrite reductase that
842 catalyses synthesis of nitric oxide and evidence from trapping experiments for nitric oxide
843 as a free intermediate during denitrifi. Eur. J. Biochem. *179*, 683–692. 10.1111/j.1432-
844 1033.1989.tb14601.x.
845 32. VoBwinkel, R., Neidt, I., and Bothe, H. (1991). The production and utilization of nitric
846 oxide by a new, denitrifying strain of Pseudomonas aeruginosa. Arch. Microbiol. *156*, 62–

847 69. 10.1007/BF00418189.
848 33. Carlson, C.A., and Ingraham, J.L. (1983). Comparison of denitrification by Pseudomonas
849 stutzeri, Pseudomonas aeruginosa, and paracoccus denitrificans. Appl. Environ.
850 Microbiol. *45*, 1247–1253. 10.1128/aem.45.4.1247-1253.1983.
851 34. Chen, J., and Strous, M. (2013). Denitrification and aerobic respiration, hybrid electron
852 transport chains and co-evolution. Biochim. Biophys. Acta - Bioenerg. *1827*, 136–144.
853 10.1016/j.bbabio.2012.10.002.
854 35. Eschbach, M., Schreiber, K., Trunk, K., Buer, J., Jahn, D., and Schobert, M. (2004).
855 Long-term anaerobic survival of the opportunistic pathogen Pseudomonas aeruginosa via
856 pyruvate fermentation. J. Bacteriol. *186*, 4596–4604. 10.1128/JB.186.14.4596-
857 4604.2004.
858 36. Glasser, N.R., Kern, S.E., and Newman, D.K. (2014). Phenazine redox cycling enhances
859 anaerobic survival in Pseudomonas aeruginosa by facilitating generation of ATP and a
860 proton-motive force. Mol. Microbiol. *92*, 399–412. 10.1111/mmi.12566.
861 37. Weinstein, B.T., Lavrentovich, M.O., Möbius, W., Murray, A.W., and Nelson, D.R. (2017).
862 Genetic drift and selection in many-allele range expansions 10.1101/145631.
863 38. Ciccarese, D., Zuidema, A., Merlo, V., and Johnson, D.R. (2020). Interaction-dependent
864 effects of surface structure on microbial spatial self-organization. Philos. Trans. R. Soc. B
865 Biol. Sci. *375*, 20190246. 10.1098/rstb.2019.0246.
866 39. Momeni, B., Brileya, K.A., Fields, M.W., and Shou, W. (2013). Strong inter-population
867 cooperation leads to partner intermixing in microbial communities. Elife *2013*, 1–23.
868 10.7554/eLife.00230.
869 40. Lancaster, J.R. (1994). Simulation of the diffusion and reaction of endogenously
870 produced nitric oxide. Proc. Natl. Acad. Sci. U. S. A. *91*, 8137–8141.
871 10.1073/pnas.91.17.8137.
872 41. Krichels, A.H., Homyak, P.M., Aronson, E.L., Sickman, J.O., Botthoff, J., Shulman, H.,
873 Piper, S., Andrews, H.M., and Jenerette, G.D. (2022). Rapid nitrate reduction produces
874 pulsed NO and N2O emissions following wetting of dryland soils. Biogeochemistry *158*,
875 233–250. 10.1007/s10533-022-00896-x.
876 42. Price-Whelan, A., Dietrich, L.E.P., and Newman, D.K. (2007). Pyocyanin alters redox
877 homeostasis and carbon flux through central metabolic pathways in Pseudomonas
878 aeruginosa PA14. J. Bacteriol. *189*, 6372–6381. 10.1128/JB.00505-07.
879 43. Dar, D., Dar, N., Cai, L., and Newman, D.K. (2021). In situ single-cell activities of
880 microbial populations revealed by spatial transcriptomics. bioRxiv, 2021.02.24.432792.

881 44. DePas, W.H., Starwalt-Lee, R., Van Sambeek, L., Kumar, S.R., Gradinaru, V., and
882 Newman, D.K. (2016). Exposing the three-dimensional biogeography and metabolic
883 states of pathogens in cystic fibrosis sputum via hydrogel embedding, clearing, and rRNA
884 labeling. MBio *7*, 1–11. 10.1128/mBio.00796-16.
885 45. Pessi, I.S., Viitamäki, S., Eronen-Rasimus, E., Delmont, T.O., Luoto, M., and Hultman, J.
886 (2020). Truncated denitrifiers dominate the denitrification pathway in tundra soil
887 metagenomes. bioRxiv. 10.1101/2020.12.21.419267.
888 46. Wilbert, S.A., Mark Welch, J.L., and Borisy, G.G. (2020). Spatial Ecology of the Human
889 Tongue Dorsum Microbiome. Cell Rep. *30*, 4003-4015.e3. 10.1016/j.celrep.2020.02.097.
890 47. Cordero, O.X., and Datta, M.S. (2016). Microbial interactions and community assembly at
891 microscales. Curr. Opin. Microbiol. *31*, 227–234. 10.1016/j.mib.2016.03.015.
892 48. Gralka, M., Szabo, R., Stocker, R., and Cordero, O.X. (2020). Trophic Interactions and
893 the Drivers of Microbial Community Assembly. Curr. Biol. *30*, R1176–R1188.
894 10.1016/j.cub.2020.08.007.
895 49. Ma, L., and Cordero, O.X. (2018). Solving the structure-function puzzle. Nat. Microbiol. *3*,
896 750–751. 10.1038/s41564-018-0186-7.
897 50. Proctor, D.M., and Relman, D.A. (2017). The Landscape Ecology and Microbiota of the
898 Human Nose, Mouth, and Throat. Cell Host Microbe *21*, 421–432.
899 10.1016/j.chom.2017.03.011.
900 51. Fuhrman, J.A. (2009). Microbial community structure and its functional implications.
901 Nature *459*, 193–199. 10.1038/nature08058.
902 52. Widder, S., Allen, R.J., Pfeiffer, T., Curtis, T.P., Wiuf, C., Sloan, W.T., Cordero, O.X.,
903 Brown, S.P., Momeni, B., Shou, W., et al. (2016). Challenges in microbial ecology:
904 Building predictive understanding of community function and dynamics. ISME J. *10*,
905 2557–2568. 10.1038/ismej.2016.45.
906 53. Kuhns, D.B., Priel, D.A.L., Chu, J., and Zarember, K.A. (2015). Isolation and Functional
907 Analysis of Human Neutrophils. Curr. Protoc. Immunol. *111*, 139–148.
908 10.1002/0471142735.im0723s111.
909 54. Kolpen, M., Kühl, M., Bjarnsholt, T., Moser, C., Hansen, C.R., Liengaard, L., Kharazmi,
910 A., Pressler, T., Høiby, N., and Jensen, P.Ø. (2014). Nitrous oxide production in sputum
911 from cystic fibrosis patients with chronic Pseudomonas aeruginosa lung infection. PLoS
912 One *9*. 10.1371/journal.pone.0084353.
913 55. Findlay, A.J., Bennett, A.J., Hanson, T.E., and Luther, G.W. (2015). Light-dependent
914 sulfide oxidation in the anoxic zone of the chesapeake bay can be explained by small

915 populations of phototrophic bacteria. Appl. Environ. Microbiol. *81*, 7560–7569.
916 10.1128/AEM.02062-15.
917 56. Prieto-Barajas, C.M., Valencia-Cantero, E., and Santoyo, G. (2018). Microbial mat
918 ecosystems: Structure types, functional diversity, and biotechnological application.
919 Electron. J. Biotechnol. *31*, 48–56. 10.1016/j.ejbt.2017.11.001.
920 57. Jungblut, A.D., Hawes, I., Mackey, T.J., Krusor, M., Doran, P.T., Sumner, D.Y., Eisen,
921 J.A., Hillman, C., and Goroncy, A.K. (2016). Microbial mat communities along an oxygen
922 gradient in a perennially ice-covered Antarctic lake. Appl. Environ. Microbiol. *82*, 620–
923 630. 10.1128/AEM.02699-15.
924 58. Zhang, I.H., Mullen, S., Ciccarese, D., Dumit, D., Martocello, D.E., Toyofuku, M., Nomura,
925 N., Smriga, S., and Babbin, A.R. (2021). Ratio of Electron Donor to Acceptor Influences
926 Metabolic Specialization and Denitrification Dynamics in Pseudomonas aeruginosa in a
927 Mixed Carbon Medium. Front. Microbiol. *12*, 1–13. 10.3389/fmicb.2021.711073.
928 59. Shanks, R.M.Q., Caiazza, N.C., Hinsa, S.M., Toutain, C.M., and O'Toole, G.A. (2006).
929 Saccharomyces cerevisiae-based molecular tool kit for manipulation of genes from gram-
930 negative bacteria. Appl. Environ. Microbiol. 10.1128/AEM.00682-06.
931 60. Spero, M.A., and Newman, D.K. (2018). Chlorate Specifically Targets Oxidant-Starved,
932 Antibiotic- Tolerant Populations of Pseudomonas aeruginosa Biofilms Melanie. MBio *9*,
933 e01400-18.
934 61. Choi, K.H., and Schweizer, H.P. (2006). mini-Tn7 insertion in bacteria with single attTn7
935 sites: Example Pseudomonas aeruginosa. Nat. Protoc. *1*, 153–161.
936 10.1038/nprot.2006.24.
937 62. Basta, D.W., Bergkessel, M., and Newman, D.K. (2017). Identification of fitness
938 determinants during energy-limited growth arrest in Pseudomonas aeruginosa. MBio *8*,
939 1–17. 10.1128/mBio.01170-17.
940 63. Meirelles, L.A., and Newman, D.K. (2018). Both toxic and beneficial effects of pyocyanin
941 contribute to the lifecycle of Pseudomonas aeruginosa. Mol. Microbiol. *110*, 995–1010.
942 10.1111/mmi.14132.
943 64. Waskom, M. (2021). seaborn: statistical data visualization. J. Open Source Softw.
944 10.21105/joss.03021.
945 65. Van Rossum, G., Drake, F.L., Harris, C.R., Millman, K.J., van der Walt, S.J., Gommers,
946 R., Virtanen, P., Cournapeau, D., Wieser, E., Taylor, J., et al. (2009). Python 3 Reference
947 Manual.
948 66. Aakanksha Wany, Pradeep Kumar Pathak, and K.J.G. (2020). Methods for Measuring

949 Nitrate Reductase, Nitrite Levels, and Nitric Oxide from Plant Tissues Aakanksha. *2057*,
950 5–6.
951 67. McBee, M.E., Chionh, Y.H., Sharaf, M.L., Ho, P., Cai, M.W.L., and Dedon, P.C. (2017).
952 Production of superoxide in bacteria is stress- and cell state-dependent: A gating-
953 optimized flow cytometry method that minimizes ROS measurement artifacts with
954 fluorescent dyes. Front. Microbiol. *8*, 1–17. 10.3389/fmicb.2017.00459.
955 68. Schindelin, J., Arganda-Carreras, I., Frise, E., Kaynig, V., Longair, M., Pietzsch, T.,
956 Preibisch, S., Rueden, C., Saalfeld, S., Schmid, B., et al. (2012). Fiji: An open-source
957 platform for biological-image analysis. Nat. Methods *9*, 676–682. 10.1038/nmeth.2019.
958 69. Bois, J. (2022). justinbois/iqplot: v0.2.0. 10.22002/D1.20286.
959
960

961

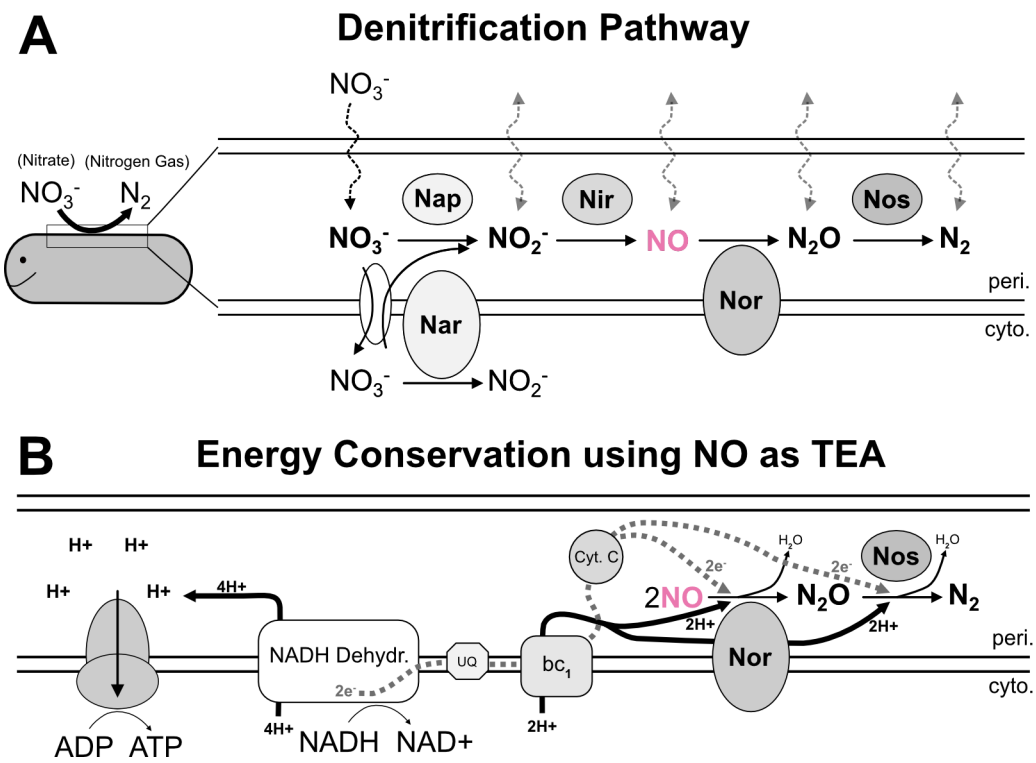
A
Denitrification Pathway
NO3-
(Nitrate)
(Nitrogen Gas)
NO3-
N2
Nap
Nir
Nos
NO3-
NO2-
NO
N2O
N2
Nar
Nor
peri.
cyto.
NO3-
NO2-
B
Energy Conservation using NO as TEA
H+
H+
H+
H+
4H+
NADH Dehydr.
2e-
UQ
bc1
Cyt. C
2e-
H2O
2e-
H2O
Nos
2NO
N2O
N2
2H+
2H+
Nor
peri.
cyto.
ADP
ATP
4H+
NADH
NAD+
2H+

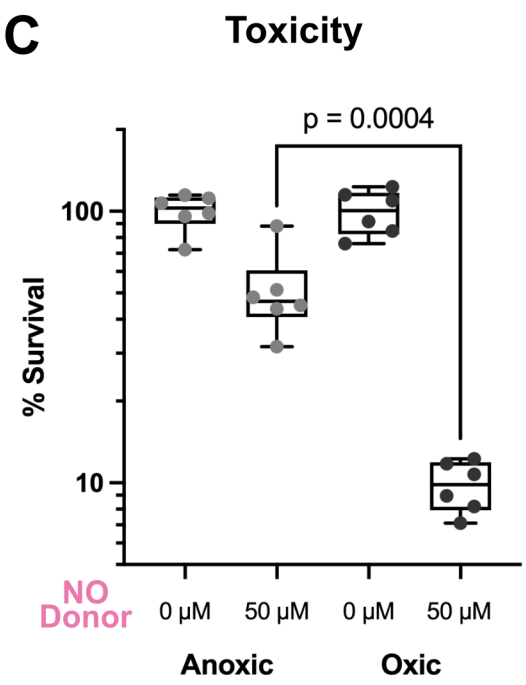
C
Toxicity
p = 0.0004
% Survival
100
10
NO Donor
0 μM
50 μM
0 μM
50 μM
Anoxic
Oxic

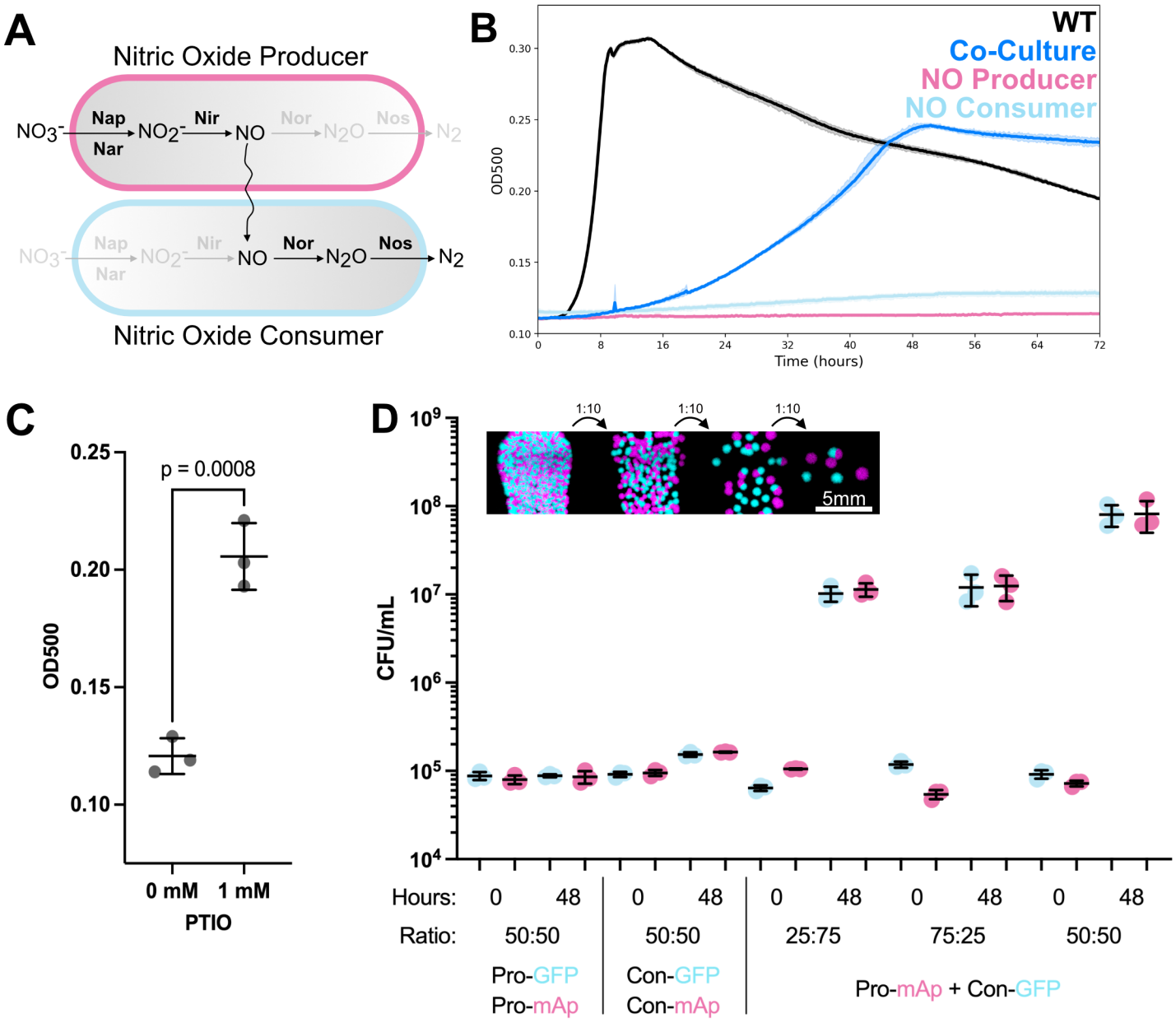
A
Nitric Oxide Producer
NO3-
Nap
Nar
NO2-
Nir
NO
Nor
N2O
Nos
N2
Nitric Oxide Consumer
B
WT
Co-Culture
NO Producer
NO Consumer
OD500
Time (hours)
C
p = 0.0008
OD500
0 mM
1 mM
PTIO
D
1:10
5mm
CFU/mL
Hours:
Ratio:
50:50
25:75
75:25
Pro-GFP
Pro-mAp
Con-GFP
Con-mAp
Pro-mAp + Con-GFP

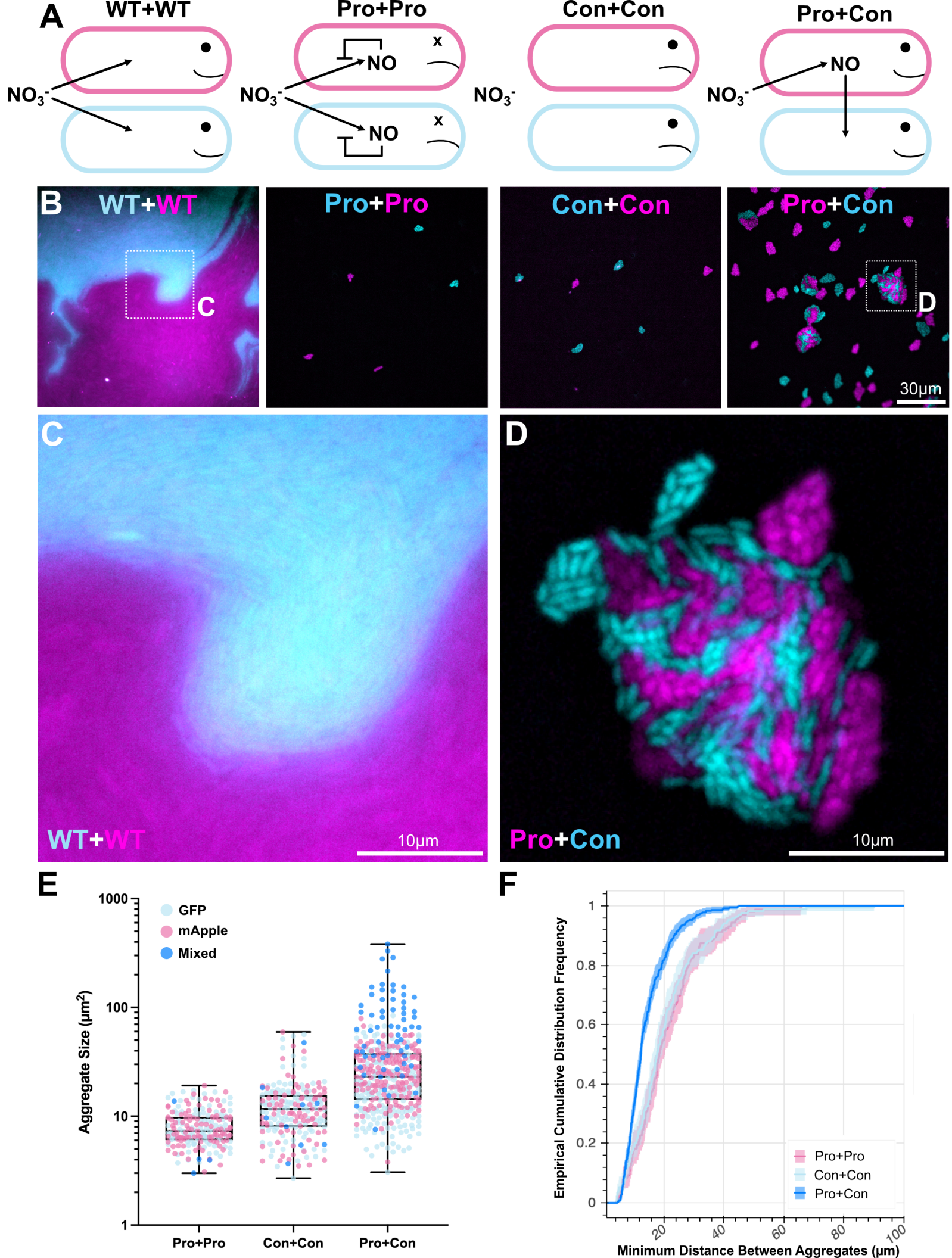
A
WT+WT
Pro+Pro
Con+Con
Pro+Con
NO_3^-
NO
x
B
WT+WT
Pro+Pro
Con+Con
Pro+Con
C
D
30μm
C
WT+WT
10μm
D
Pro+Con
10μm
E
GFP
mApple
Mixed
Aggregate Size (μm²)
1000
100
10
1
Pro+Pro
Con+Con
Pro+Con
F
Empirical Cumulative Distribution Frequency
1
0.8
0.6
0.4
0.2
0
20
40
60
80
100
Minimum Distance Between Aggregates (μm)
Pro+Pro
Con+Con
Pro+Con

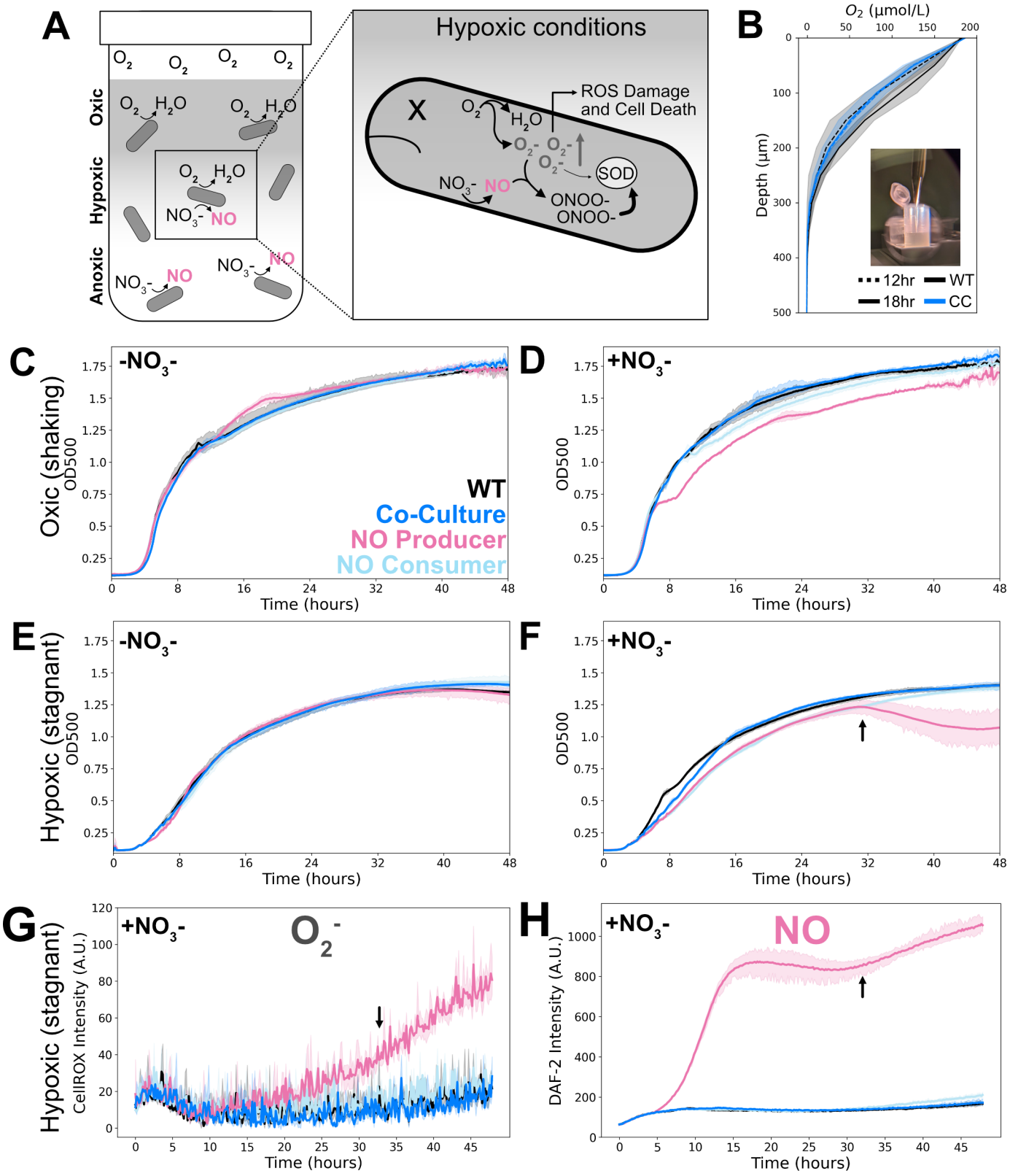
A
Oxic
Hypoxic
Anoxic
Hypoxic conditions
ROS Damage and Cell Death
SOD
ONOO-
B
O_2 (µmol/L)
Depth (µm)
12hr
18hr
WT
CC
C
-NO_3-
Oxic (shaking)
OD500
Time (hours)
WT
Co-Culture
NO Producer
NO Consumer
D
+NO_3-
E
-NO_3-
Hypoxic (stagnant)
F
+NO_3-
G
+NO_3-
O_2^-
CellROX Intensity (A.U.)
H
+NO_3-
NO
DAF-2 Intensity (A.U.)

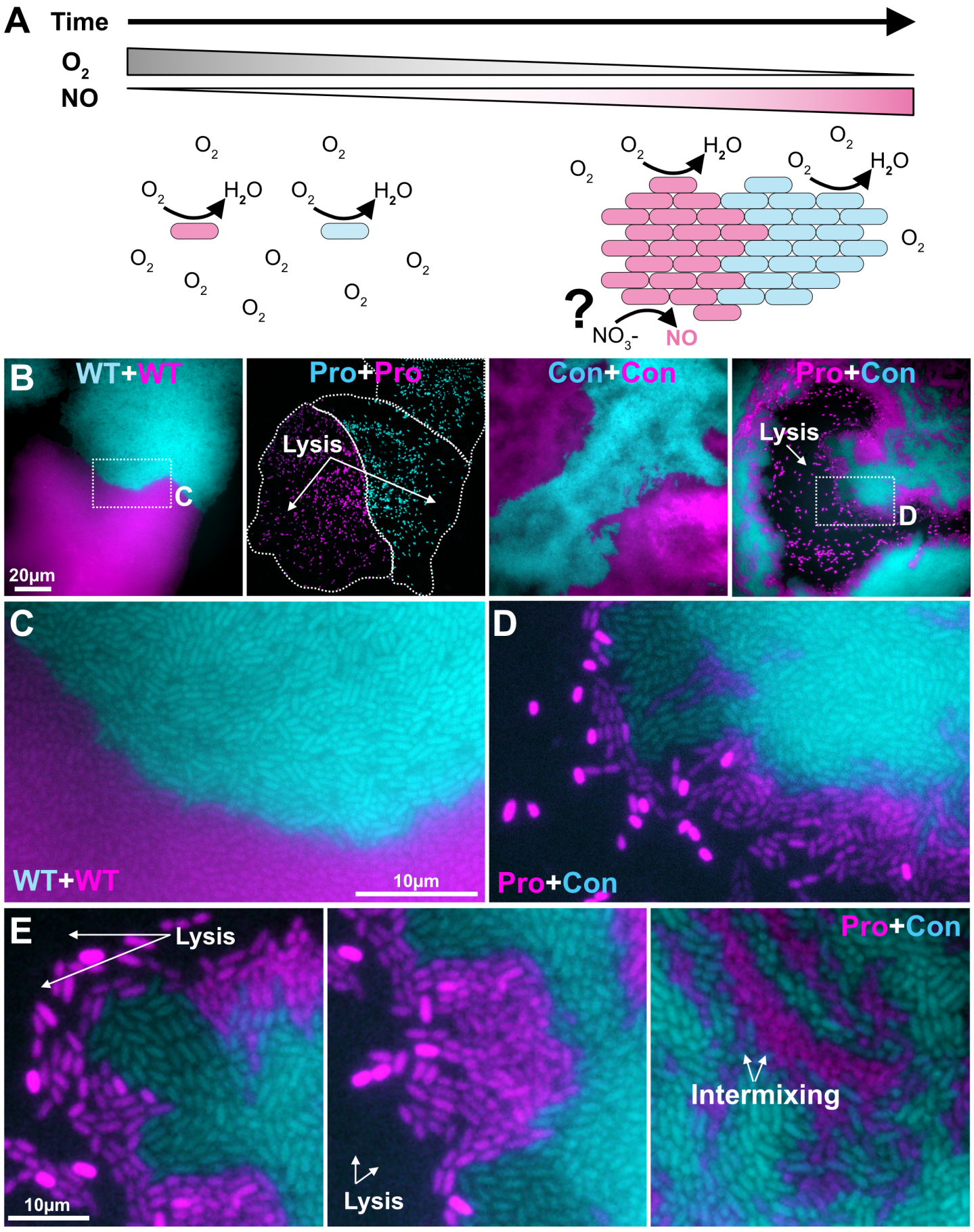

Protection from lysis following consumer contour

Protection from lysis in consumer pocket

Protection from lysis by intermixing

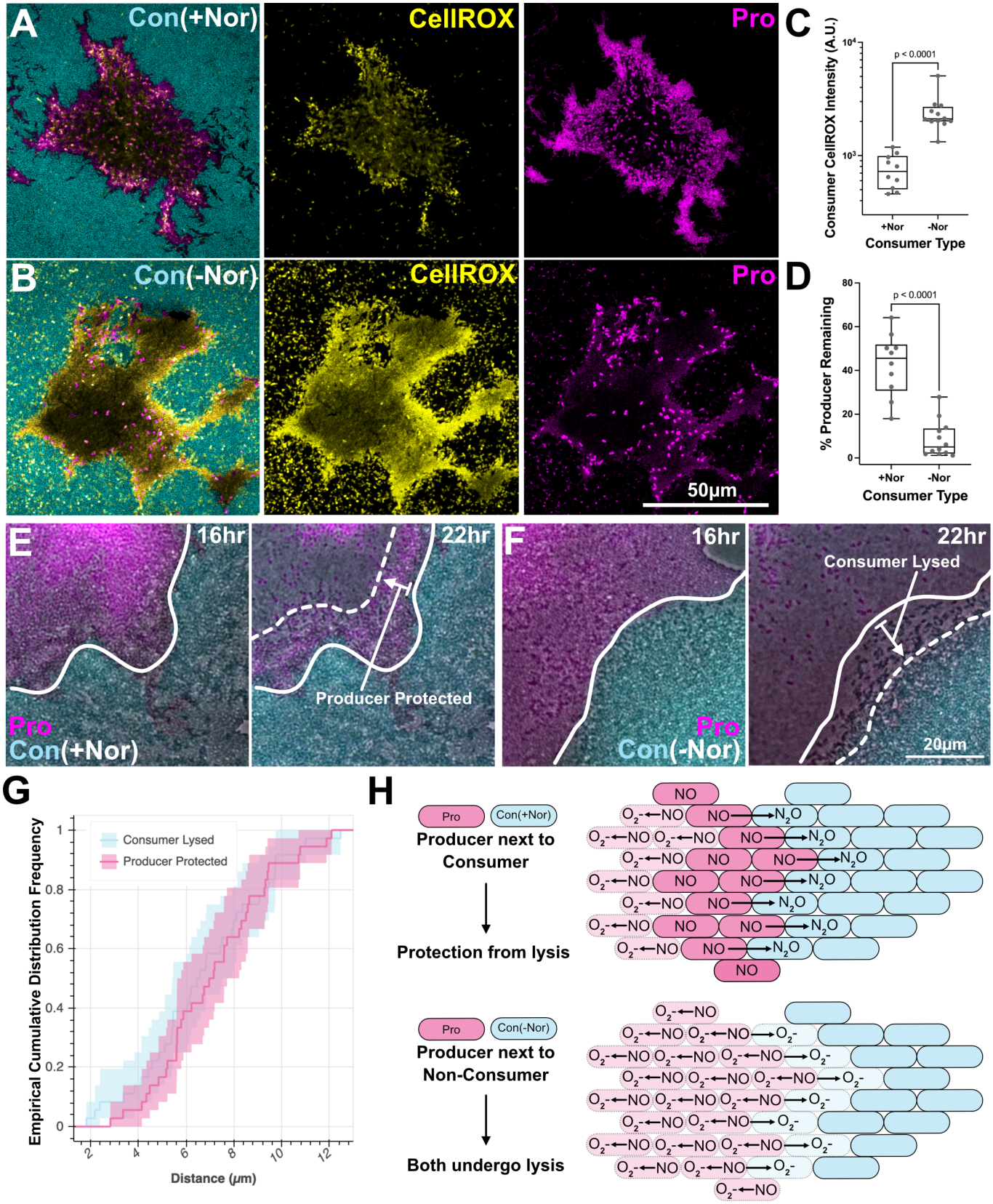
A
Con(+Nor)
CellROX
Pro
B
Con(-Nor)
CellROX
Pro
50µm
C
Consumer CellROX Intensity (A.U.)
p < 0.0001
+Nor
-Nor
Consumer Type
D
% Producer Remaining
p < 0.0001
+Nor
-Nor
Consumer Type
E
16hr
22hr
Producer Protected
Pro
Con(+Nor)
F
16hr
22hr
Consumer Lysed
Pro
Con(-Nor)
20µm
G
Consumer Lysed
Producer Protected
Empirical Cumulative Distribution Frequency
Distance (µm)
H
Pro
Con(+Nor)
Producer next to Consumer
Protection from lysis
Pro
Con(-Nor)
Producer next to Non-Consumer
Both undergo lysis